43rd AIAA Aerospace Sciences Meeting and Exhibit
10-13 Jan 2005 Reno, Nevada

AIAA-2005-0210

Noise and Spreading of a Subsonic Coannular Jet – Comparison with Single Equivalent Jet

K. B. M. Q. Zaman* and M. D. Dahl†

NASA Glenn Research Center, Cleveland, OH 44135

The issue of scaling of noise as well as spreading of subsonic coannular jets is revisited. Far-field noise and centerline Pitot-static pressure surveys are conducted with concentric, circular nozzles having an outer-to-inner diameter ratio of 1.42. Both the inner nozzle and the outer annular passage are convergent. Outer-to-inner Mach number ratio (*R*) is varied over a large range from 0 to approximately 10. Results are examined on the basis of single equivalent jet parameters calculated by satisfying continuity, momentum and energy equations. The results confirm that coannular jets with 'normal' velocity profiles are noisier than the single equivalent jet. Jets with 'inverted' velocity profiles are also found to be noisier except in a narrow *R*-range of 1-1.5. In the latter range, contrasting the inference in previous studies of IVP jets, the present data do not exhibit a clear noise reduction. When normalized with equivalent jet parameters the asymptotic Mach number decay rate, as well as potential core length, are found to be comparable to those of a single jet. However, an abrupt shift in the virtual origin is noted across *R*=1.

1. Introduction

This study was prompted by earlier investigations of noise reduction with offset (eccentric) coannular nozzles.[1,2] The reduction of noise was measured relative to that of the corresponding concentric configuration. For the latter basic configuration, some questions came up regarding the scaling of the noise vis-à-vis the noise of a 'single equivalent jet'. These are addressed in this paper with the help of experimental data from a concentric coannular nozzle having convergent inner as well as outer annular flows.

For a given primary jet, it has been known that the onset of the outer annular flow attenuates noise when measured at a fixed microphone location.[3,4] However, thrust and mass flow rate also change with the addition of the annular flow. Those must be accounted for in order to assess the net impact on the noise field relative to that of a single equivalent jet. The issue was addressed, among others, by Tanna.[4] He reached the inference that coannular jets are in fact noisier for normal velocity profiles (i.e., inner jet having higher velocity) but quieter for a range of conditions for inverted velocity profiles (i.e., inner jet having lower velocity).

The assumptions made in the determination of the single equivalent jet (referred in the following as SEJ, after Ref. 5), however, have not been reviewed critically. In Ref. 4, a constant area assumption was invoked in addition to satisfying continuity and momentum equations. That is, the exit area of the SEJ was assumed to be the same as the exit area of the outer nozzle. A detailed analysis for noise prediction was carried out in Ref. 5; a constant area assumption was also invoked for obtaining the SEJ parameters for the merged flow region of the jet. In Refs. 6 and 7, a further comprehensive analysis was carried out for correlation and prediction of coannular jet noise. The analysis drew on experimental results of the flow-field, e.g., reported in Ref. 8. The equivalent jet was defined differently for different flow regimes, to be discussed further in the text. In Ref. 9 as well as Ref. 7, while analyzing heated jet data, enthalpy conservation was also satisfied besides continuity and momentum for obtaining the SEJ parameters. Even though the present experiment involves 'cold' flow (that is, the total temperature was constant throughout and equal to that in the ambient), the data analysis is carried out on the latter, more rigorous, basis. The constant area procedure is also considered to examine the impact on the results.

---

* Aerospace Engineer, Propulsion Systems Division, Nozzle Branch, Mail Stop 86-7, Associate Fellow AIAA.
† Aerospace Engineer, Propulsion Systems Division, Acoustics Branch, Mail Stop 54-3, Member AIAA.
This material is declared a work of the U.S. Government and is not subject to copyright protection in the United States.

This is a preprint or reprint of a paper intended for presentation at a conference. Because changes may be made before formal publication, this is made available with the understanding that it will not be cited or reproduced without the permission of the author.

Coannular jets are known to spread more slowly. With the addition of the annular flow the potential core of the primary jet extends farther downstream. Again, similar considerations come into play and one may ask how these characteristics, when viewed in terms of the SEJ, would compare with single jet measurements. In this investigation we define the SEJ based on full set of conservation equations and also review the impact of various simplifications. The overall intensity and spectra of the far-field noise, covering a wide range of velocity ratios, are analyzed first. Jet spreading, based on centerline Mach number decay, is then examined in the light of the SEJ parameters.

2. Experimental Facility

Figure 1 shows the open jet facility in which the experiment was conducted.[2] Here, only the inner (primary) nozzle is visible, directly attached to the 30 in. diameter main plenum chamber. Another annular plenum chamber, located just upstream of the nozzles, provided the outer (secondary) flow. The outer flow, supplied by four equally spaced ports, was routed through contoured interior and screens to provide a uniform velocity profile at the exit. Flow uniformity was confirmed by Pitot probe surveys.[2] For the present experiment, the inner nozzle was convergent with an exit diameter of 1.48 in. and a lip thickness of 0.03 in. The outer annular passage was also convergent. The diameter of the outer nozzle (D_o) was 2.1 in. The nozzles were essentially 'coplanar' with the inner nozzle lip protruding 0.125 in. relative to the exit of the outer nozzle. The ratio of primary-to-annular exit area was 0.92.

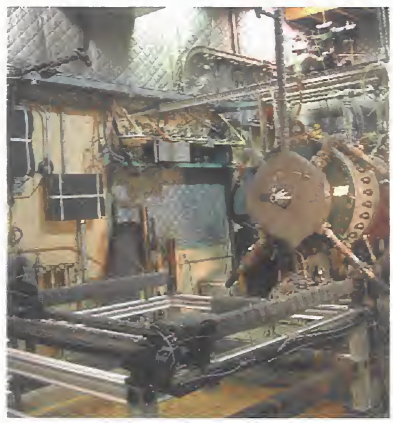

Fig. 1 Jet facility.

In the following, the subscripts '*1*' and '*2*' denote conditions in the inner jet and the outer annular flows, respectively. The subscript '*o*' is used to denote the outer nozzle diameter. Subscripts '*eq*' and '*a*' represent equivalent jet and ambient conditions, respectively. The parameter R ($=M_2/M_1$) is the ratio of the two Mach numbers at the exit of the nozzle. Subsonic flow, ensuring shock-free operation in both streams, was ensured for all results presented in this paper.

Pitot-static probe surveys were conducted on the axis of the jet over the x/D_O range, -0.2 – 26.3. The probe had a 0.065 in. outer diameter with static ports located 0.39 in. from the tip. For approximately $x/D_O > 5$, the measured static pressure was assumed to apply at the Pitot location, for calculation of Mach number. Close to the nozzle, because of sharper gradients, separate static pressure runs were done to match the locations of Pitot pressure data. With each data (flow as well as noise), the two mass-flow rates and plenum pressures were recorded simultaneously. Since the cross-sectional area ratio was 0.92 the bypass ratio was close to R. Only R is quoted with all data presented in the following.

2.1 Noise data

The far-field noise was measured with (B&K model 4135) microphones located at $37.1D_1$ and $50.2\ D_1$ from the nozzle exit for θ =25° and 90°, respectively. The polar location θ was measured relative to the downstream jet axis. Spectral analysis of the microphone signal was done by a Nicolet 660B analyzer. The entire test chamber had sound absorbing 'baffles' on the ceiling and 'coatings' on the upper half of all four walls. For this experiment, the floor and other exposed surfaces in the vicinity of the facility were wrapped with sound absorbing material. Nevertheless, the picture in Fig. 1 should indicate that the environment was far from ideal for noise measurement. Thus, an assessment of the quality of the noise data was desired.

Figure 2 shows power spectral density for the primary jet only, compared to data from a few other facilities. These include a set of data from the aeropropulsion laboratory ('dome') at GRC (Dr. James Bridges, private communication,[10]) a set from UC-Irvine (Dr. Dimitri Papamoschou, private communication,[1])and another one from an experiment at Boeing Seattle facilities (Dr. K. Viswanathan, private communication,[11]). The reference 'Z&Y' stands for earlier experiments in the anechoic flow facility of NASA Langley.[12] The nozzle diameters (in inches) and jet Mach numbers are indicated in the legends; 'atm-c' indicates that correction for atmospheric attenuation has been performed.[13] The sound power spectral density (PSD) is normalized as,[12]

$$P^* = (p'/\rho_j U_j^{\,2})^2 (r/D)^2 (U_j/(\Delta f D)). \qquad (1)$$

Here, p' is the r.m.s. pressure fluctuation in the frequency band Δf, and ρ_j, U_j and M_j represent the density, velocity and Mach number at the nozzle exit; D is the nozzle diameter and r the distance of the measurement location from the exit of the nozzle. (An astute reader should note that for simplicity ρ_a was substituted for ρ_j in Ref. 12). The rationale for scaling P^* with $M_j^{5.5}$ at shallow angles, and with $M_j^{3.5}$ at 90°, is based on correlation of several sets of noise data available at the time of the cited investigation. The adopted scaling yielded the best collapse of the data. This implied a $U^{8.5}$- and a $U^{6.5}$-scaling for the spectral amplitudes at θ=25° and 90°, respectively.

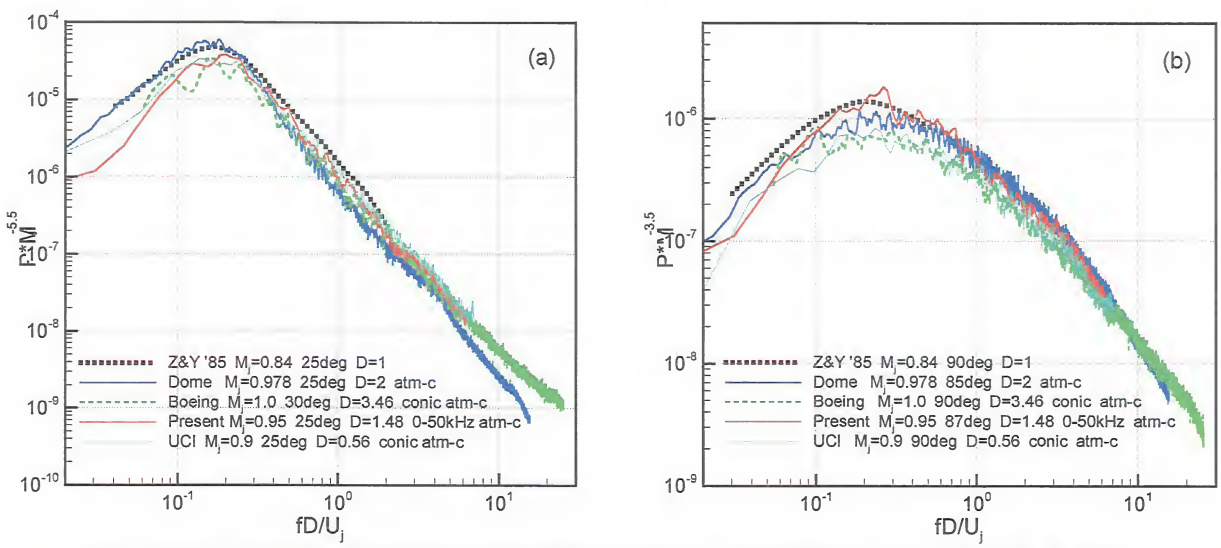

Fig. 2 Noise power spectral density compared to data from other facilities: (a) θ = 25°, (b) θ = 90°.

First, let us consider the data from the other facilities in Fig. 2. The normalized PSD have collapsed reasonably. The Boeing data involve the largest nozzle and has some undulations on the low frequency end. The UCI data are with the smallest nozzle and reflect fine quality. However, there are differences that may not be insignificant. Note that P^* represents $(p')^2$ and thus each decade on the ordinate represents 10 dB in SPL. The scatter near the spectral peak is about 1.5 dB. Away from the peak the amplitude scatter may be more. It is emphasized that 'scatter' in this context refers to variations in data from different facilities and not data repeatability in a given facility. It is near impossible to identify all sources contributing to the scatter. Apart from differences in test chamber conditions and 'internal noise', simply the hardware geometry can have an impact. In the Boeing experiment,[11] more than 2 dB difference occurred (on high frequency end) with two nozzles having different internal contours (ASME profile versus conic) with all other test conditions remaining the same. Data from the conic nozzle is shown in Fig. 2; the ASME nozzle was noisier. It remains unclear how nozzle geometry factors in. Besides influencing transmission of internal noise another possibility is via a difference in the exit boundary layer characteristics. In the GRC experiment, nozzle size as well as boundary layer state made a difference (Ref. 10; see also Ref. 14). The upshot is that about 2 dB scatter is still the reality in jet noise data quality, although this is a significant improvement since Ref. 12 when more than 5dB scatter was noted.

Figure 2 shows that the present data fall reasonably close to the scatter band. In fact, the agreement is surprisingly good in view of the imperfect test chamber conditions. The most notable disagreement is the lower amplitude on the low frequency end in Fig. 2(a) and a bump near the peak in Fig. 2(b). The reasons remain unexplored. Nevertheless, the data quality was considered adequate for the comparative investigation at hand. All spectral data in the following were obtained with same bandwidth (0-50kHz) and same averaging period (45 sec.).

3. Results and Discussion

Sound pressure level spectra were measured for different combinations of M_1 and M_2. The overall intensities, obtained by integration of the spectra, are shown in Figs. 3(a) and 3(b) for θ =25° and 90°, respectively. There are four sets of data: (1) $M_1 \approx 0.96$ with varying M_2, (2) $M_2 \approx 0.99$ with varying M_1, (3) $M_1 \approx 0.79$ with varying M_2, (4) $M_2 \approx 0.72$ with varying M_1. A 5th set of data is included in Fig. 3(a) for $M_1 \approx 0.61$. For set 2 ($M_2 \approx 0.99$) an additional data point at large R is shown – disconnected, since the primary pressure was at the limits of the transducer range and hence the accuracy of R was poor. The case, R=• (M_1=0), has been excluded since it appeared abnormally noisy possibly due to excitation of plenum chamber resonances (further addressed with flow data). In Fig. 3(a), for R<1, trends as reported in Refs. 3 and 4 can be seen: as R increases the intensity first decreases, reaches a minimum at $R \approx 0.5$ and then increases. For $M_2 \approx$ constant cases, a steep initial drop in intensity occurs with increasing R. For R >2.5 the intensity increases again. Corresponding data for θ =90°, shown in Fig. 3(b), exhibit similar trends. These intensity data are analyzed on the basis of equivalent jet parameters in the following.

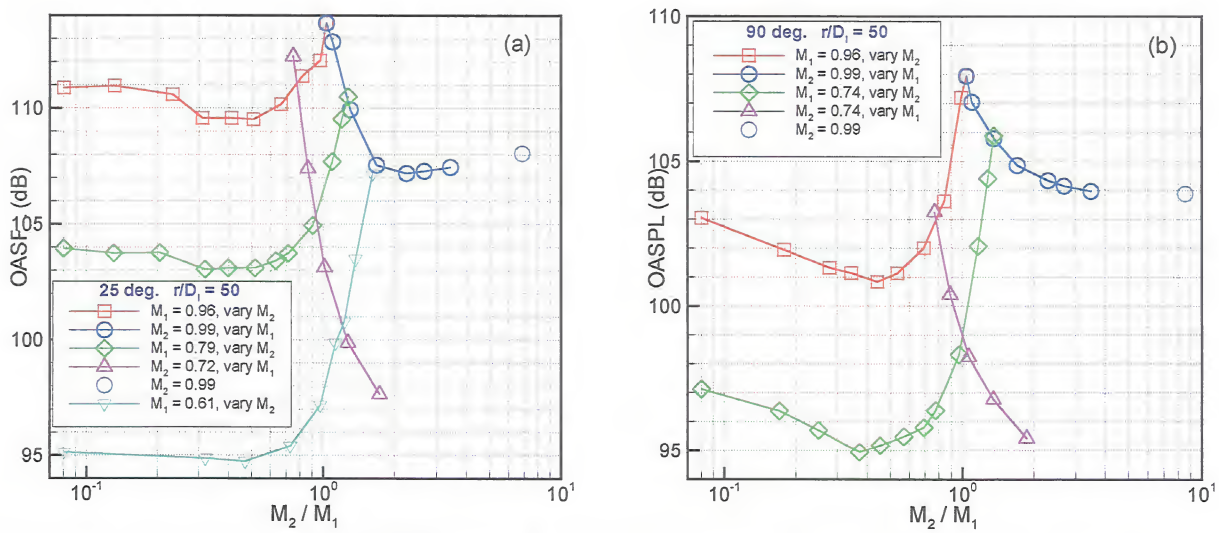

Fig. 3 Overall sound pressure level (OASPL) versus R for indicated run conditions; (a) $\theta = 25°$, (b) $\theta = 90°$.

3.1 Single equivalent jet parameters

The SEJ parameters are calculated with the assumption of 'top-hat' velocity profiles at the nozzle exit. For the static pressure at the exit, equation of state, and conservation of mass, momentum and enthalpy the following equations can be written,

$$p_{eq} = p_a, \qquad (2)$$

$$p_{eq} = \rho_{eq} R t_{eq}, \qquad (3)$$

$$\rho_1 A_1 U_1 + \rho_2 A_2 U_2 = \rho_{eq} A_{eq} U_{eq}, \qquad (4)$$

$$\rho_1 A_1 U_1^2 + \rho_2 A_2 U_2^2 = \rho_{eq} A_{eq} U_{eq}^2 \qquad (5)$$

$$T_a = t_{eq} + \frac{U_{eq}^2}{2C_p}. \qquad (6)$$

Here, p, ρ, t, T, A and U are pressure, density, static temperature, total temperature, exit area and velocity, respectively. Note that Eq. (6) is sufficient for the present case since the total temperature is the same in both streams and equal to that in the ambient. It states that the specific stagnation enthalpy in the equivalent jet is the same as everywhere else. With dissimilar temperatures one would require the full enthalpy conservation equation,[9]

$$\rho_1 A_1 U_1 T_1 + \rho_2 A_2 U_2 T_2 = \rho_{eq} A_{eq} U_{eq} T_{eq}. \qquad (7)$$

From Eqs. (2)-(6), the five unknowns, p_{eq}, ρ_{eq} , A_{eq}, U_{eq} and t_{eq}, are solved for a given pair of driving pressures for the inner and outer flows.

With the 'constant area' assumption, Eq. (6) or (7) may be replaced with,

$$A_1 + A_2 = A_{eq} . \qquad (8)$$

Equations (2)-(5) and (8) provide the SEJ parameters with the constant area assumption. For the present nozzle geometry, the quantities D_{eq}, M_{eq} and t_{eq} are calculated following either procedure and shown in Figs. 4(a), (b) and (c), respectively, as functions of R.

The parameters calculated with constant area assumption are shown by the blue curves. Naturally, D_{eq} is a constant for this case. The equivalent Mach number is a maximum at R=1 and falls off monotonically on either side. The static temperature is minimum at R=1. Away from R=1 on either side the temperature continues to increase.

The parameters obtained with constant enthalpy assumption are shown by the red curves. One finds that D_{eq} is the maximum at R=1 and decreases on either side. The limiting value of D_{eq} is D_1 at R=0 and it is equal to the equivalent diameter of the outer annulus at R=•. Ideally, D_{eq} should be equal to D_o at R=1 but it is somewhat less due to the lip thickness of the inner nozzle. M_{eq}, on the other hand, reaches minima at about R=0.5 as well as 2.5, where noise intensities are noted to have minima (Fig. 3a). The static temperature now has 'realistic' values, with maxima where M_{eq} has minima. Unless stated specifically, D_{eq} and M_{eq} obtained with the constant enthalpy assumption are used in the following. The SEJ parameters, considered in references 6 and 7, will be discussed with the spectral data in §3.3.

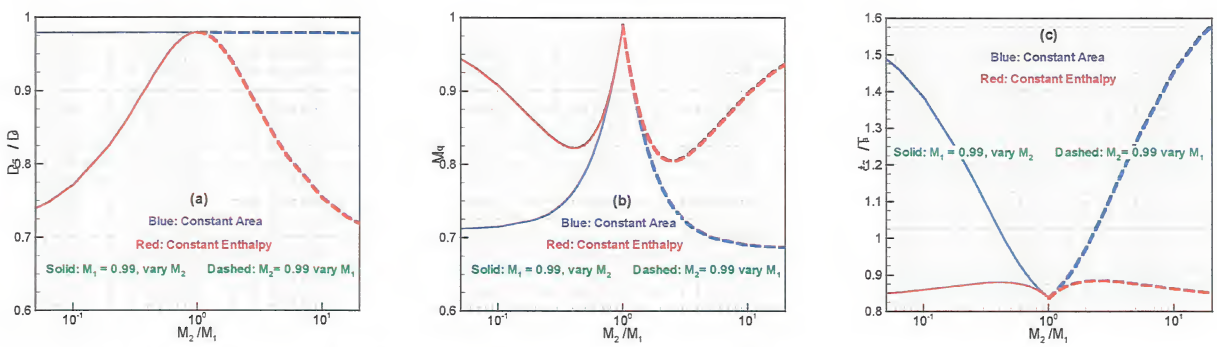

Fig. 4 Single equivalent jet parameters versus R; (a) diameter, (b) Mach number and (c) temperature.

3.2 Scaling of overall intensity data

The intensity data of Figs. 3(a) and (b) are normalized by D_{eq} and M_{eq} and shown in Figs. 5(a) and (b), respectively. Normalization with equivalent diameter has been done so as to refer the data at r/D_{eq} = 50. Normalization with Mach number involves a scaling by M_{eq}^{E}. That is, IM_{eq}^{E} $(r/ D_{eq}*50)^2$ is plotted in Fig. 5, I being the measured OASPL. The exponent E is taken to be -8.5 and -7.5 at θ=25° and 90°, respectively. The rationale was touched upon in §2. More specifically, the amplitude of the spectra scaled with exponents -8.5 and -6.5 at θ=25° and 90°, respectively. The frequency, on the other hand, scaled with ambient speed of sound (Helmholtz number scaling) and jet velocity (Strouhal number scaling) at θ=25° and 90°, respectively.[12] This led to the choice of the exponents for normalization of I.

The apparently disparate sets of data of Fig. 3(a) have collapsed quite well in Fig. 5(a). The single jet from the inner nozzle is represented at R=0 (shown arbitrarily at R=0.08 to fit in the log scale). The condition R=1 also represents a single jet except for the effect of the thin lip of the inner nozzle. Before commenting on the amplitudes at other values of R, we note that the normalized intensity is somewhat lower at R=1 than that at R=0. The reason for this is not clear; however, recall the discussion of data 'scatter' with Fig. 2. Here, the difference is about 1.5 dB for most of the data which is within the observed scatter. This could arise from differences in the upstream geometry of the nozzles. The contraction ratio and contours for the inner and outer nozzles are different; recall the nozzle geometry effect observed in Ref. 11. Nevertheless, the trend for R-range of 0-1 (normal velocity profile) is unambiguous. There, as inferred by Tanna,[4] the coannular jet is noisier. A similar observation is made from the data at θ = 90° (Fig. 5b) for this R-range.

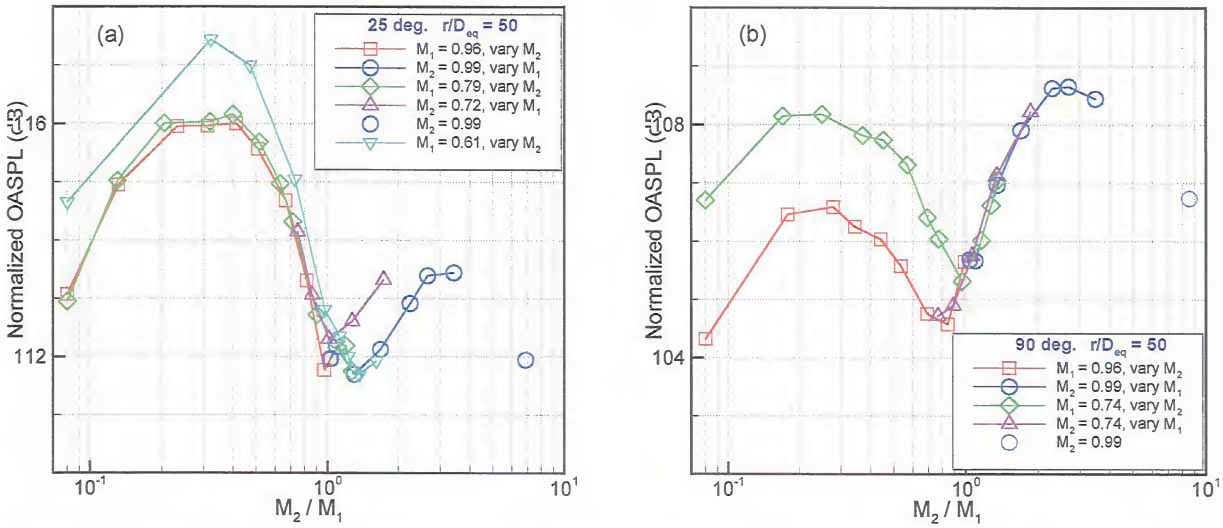

Fig. 5 OASPL data of Fig. 3 normalized by equivalent jet parameters (constant enthalpy); (a) $\theta = 25°$, (b) $\theta = 90°$.

It should be noted that in most previous studies noise comparison was made in a somewhat different manner. Typically, the measured intensity was plotted versus velocity ratio and another curve was plotted to represent the expected intensity for the SEJ. The latter curve was obtained by calculating the SEJ at each operating point and predicting its noise from available correlations (e.g., SAE code used in Ref. 9). The difference between the two curves indicated noise increase or decrease. Here, we chose to present the data simply after normalization by the SEJ parameters. The noise intensity of the SEJ is represented at R=0 or R=1. Comparison with the level at either R identifies the increase or decrease in the noise. This is a direct comparison without need for others' data or prediction code. Also, this way the impact of data 'scatter' in the comparison is kept in perspective.

The normalized intensity in both Figs. 5(a) and (b) are also found to be generally high for R>1 (inverted velocity profile). It reaches a maximum in the R-range of 2-3. The present data contrast earlier inferences that IVP jets are quieter.[4,5,9] This is further examined in Fig. 6. The θ=25ϒdata are normalized by equivalent jet parameters using the constant area assumption and plotted as a function of the velocity ratio, as done in Ref. 4. Note that U_2 /U_1 is not significantly different from R at these subsonic conditions; thus, for brevity, we will continue to use the notation R to describe the abscissa of Fig. 6. In Fig. 6(a), the full set of data corresponding to Fig. 5(a) is shown with logarithmic abscissa. First, we note that the normalized amplitude reaches a maximum at R =0. It also continues to increase as R increases on the right hand side. The increasing levels with R ♦ 0 and R♦ × follow from the M_{eq}^{E}-scaling and the fact that M_{eq} keeps on decreasing in both limits (blue curves, Fig. 4b). This underscores an intrinsic flaw with the constant area assumption. The normalized intensities of a single equivalent jet at R = 0, 1 or × are predicted different whereas ideally they should be the same. Here, only at R=1 the energy balance is also satisfied. Thus, a meaningful comparison can only be made with the SEJ at R=1.

For some of the curves in Fig. 6(a) the level continues to drop past R=1, as R increases. This is further scrutinized by zooming into the range near R=1, in Fig. 6(b). For clarity only two cases are shown. We recall that noise reduction was inferred in Refs. 4,5,9 for the approximate R-range of 1-2. This is borne out by the case shown by the blue inverted triangles. For comparison the blue horizontal line is drawn through the level at R=1 for this case. Lower intensity is observed approximately over 1< R <1.5. However, the decrease, relative to the intensity at R=1, is less than a dB. This is within the 'scatter' discussed earlier. In fact, for three out of five cases of Fig. 6(a), e.g., the one shown by the red triangles in Fig. 6(b), the level is the lowest at R=1. Thus, the present nozzle and run conditions do not affirm clear noise suppression with the IVP jets. Note that this observation is not contingent upon the procedure for obtaining the SEJ; the same trends exist in the data shown in Fig. 5(a). Note furthermore from Fig. 5(b) that none of the cases at θ =90ϒexhibit lower noise for R>1. Thus, for the conditions in the present experiment, one might infer that a single jet with top-hat velocity profile is the quietest and any nonuniformity introduced by the coannular configuration leads to higher overall noise.

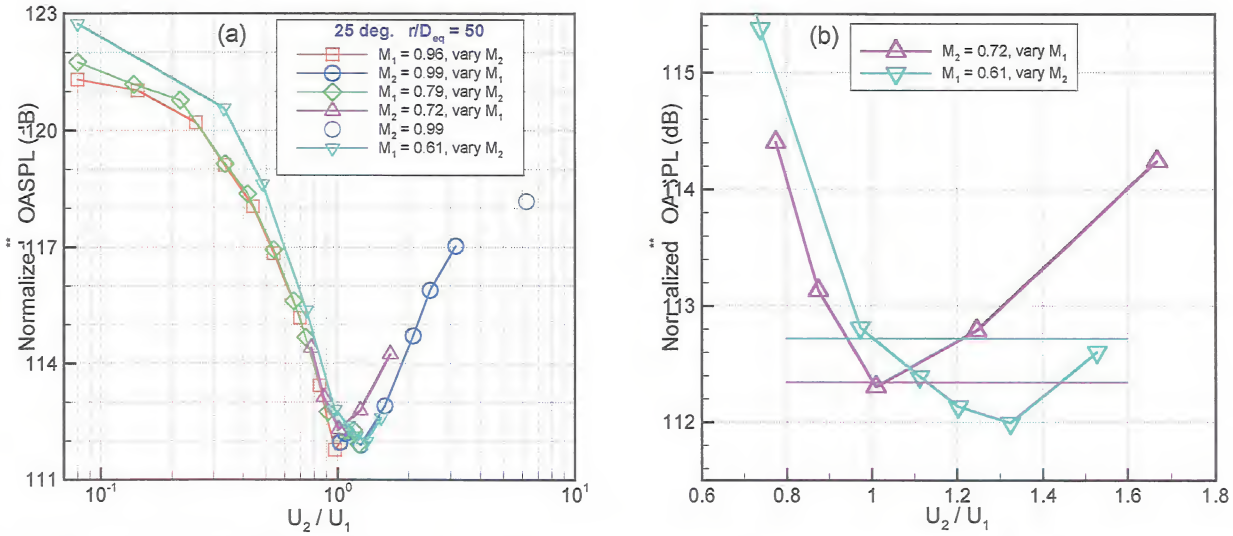

Fig. 6 Normalized OASPL ($\theta = 25°$) versus velocity ratio: (a) data in full range of abscissa (Fig. 5a), (b) data around velocity ratio of unity. (**Equivalent jet parameters based on constant area.)

3.3 Spectral data

The measured spectra are presented in Fig. 7 for θ=25°. For clarity data for R<1 and R>1 are shown separately in Figs. 7(a) and (b), respectively. Recall that the overall intensity first decreases with increasing R reaching a minimum around R=0.5 (Fig. 3a). The spectra in Fig. 7(a) reveal that the energy at low frequencies actually increases at first with increasing R; the decrease in overall intensity comes from a reduction of energy near the peak and high frequencies. At R≈1 the amplitudes are larger over the entire bandwidth. In Fig. 7(b), all the traces on the high frequency end are conspicuously congruent. This suggests that the high frequency noise for these (IVP) cases, with fixed M_2, comes from the outer shear layer that remains invariant. A similar observation in Ref. 6 led to the assumption of different SEJ for different flow regimes, as discussed shortly. Increasing M_1 (decreasing R) in Fig. 7(b) progressively increases the low frequency energy. There is also a continual decrease in the frequency of the peak with decreasing R. Corresponding data for θ=90° are shown in Figs. 8(a) and (b), and essentially similar observations can be made.

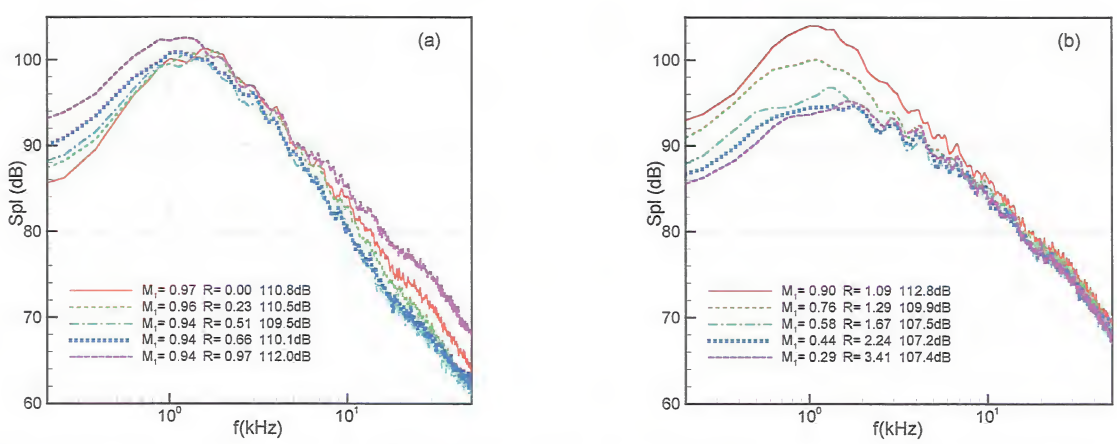

Fig. 7 Sound pressure level spectra at $\theta = 25°$. (a) $M_1 \approx 0.95$, R varying in the range 0 – 1, (b) $M_2 \approx 0.99$, R varying in the range 1 - 3.5.

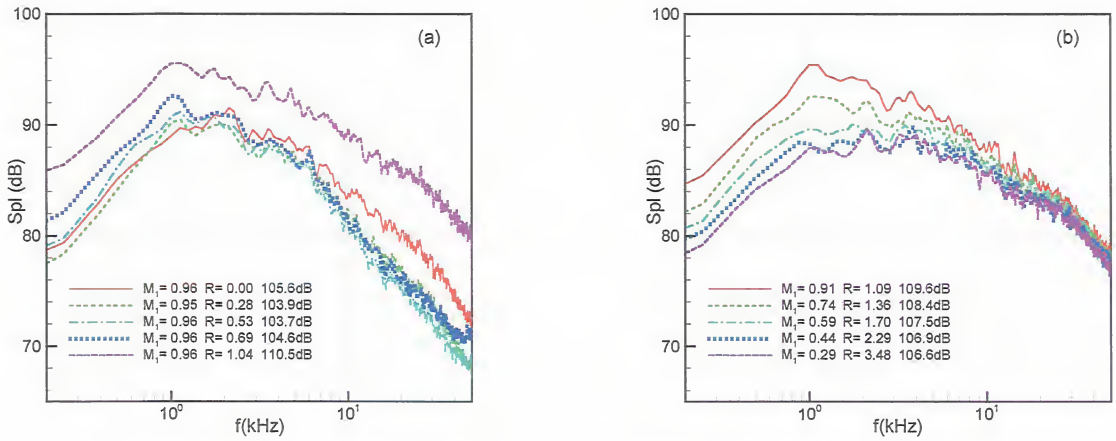

Fig. 8 Sound pressure level spectra at $\theta = 90°$. (a) $M_1 \approx 0.95$, R varying in the range 0 – 1, (b) $M_2 \approx 0.99$, R varying in the range 1 - 3.5.

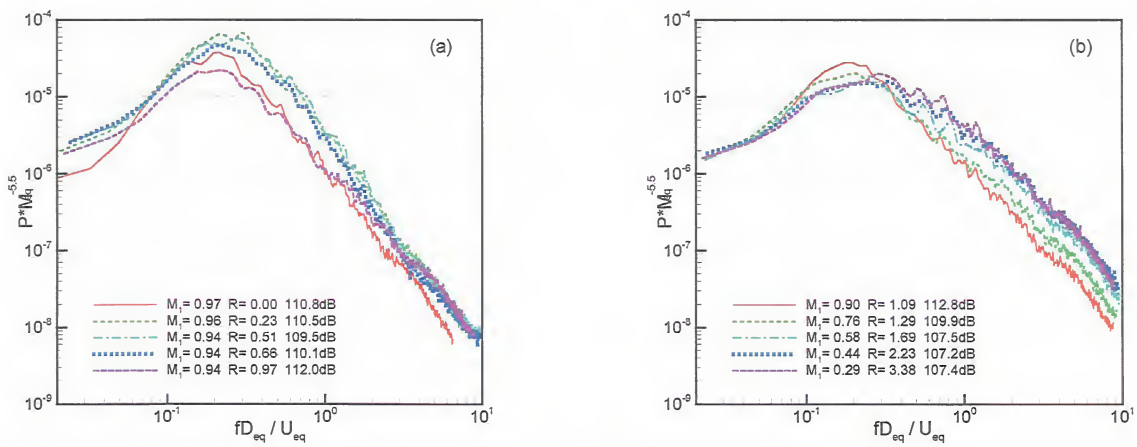

Fig. 9 Sound pressure level spectra of Fig. 7 ($\theta = 25°$) normalized by equivalent jet parameters.

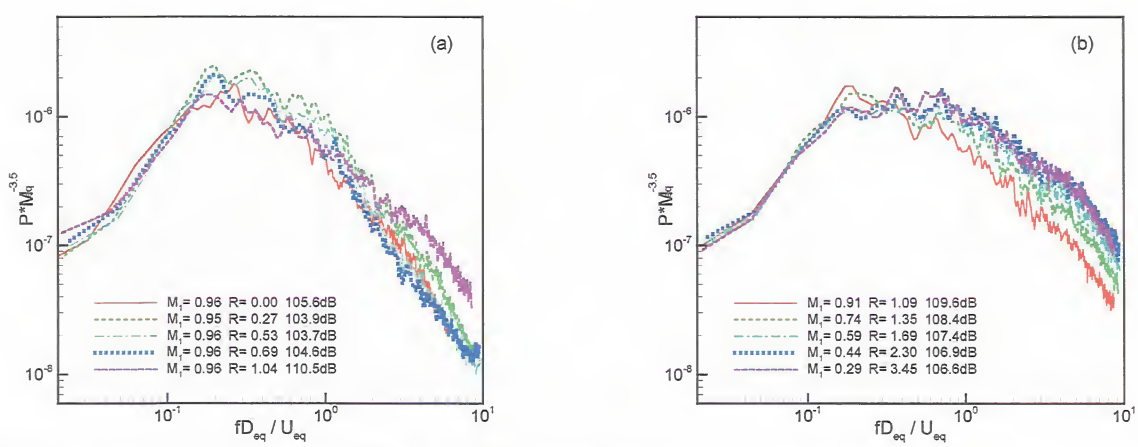

Fig. 10 Sound pressure level spectra of Fig. 8 ($\theta = 90°$) normalized by equivalent jet parameters.

The spectral data of Figs. 7 and 8 are plotted in Figs. 9 and 10, respectively, in the format of Fig. 2; D_{eq} and M_{eq} are used for the normalization. It can be seen in Fig. 9(a) that the levels are the lowest for R=0 and 0.97 (single jet cases). The amplitudes are high over the entire bandwidth at intermediate values of R, consistent with high intensities observed in Fig. 5(a). For R>1 in Fig. 9(b), the traces on the low frequency end have now collapsed, at the

'expense' of dispersion of the curves at higher frequencies that were congruent in Fig. 7(b). In particular for the IVP cases, it is as if the outermost shear layer determines the high frequency energy while the equivalent jet parameters govern the low frequency energy. This was addressed in the analysis of Ref. 6, as discussed next. Again, similar observations can be made from the θ=90° data shown in Figs. 10(a) and (b).

The spectral data underscore that it may not be possible to represent the noise from a coannular jet with that of a single equivalent jet. Scaling is different for different noise producing regions of the flow. This was considered earlier in Ref. 5 and more thoroughly in references 6 and 7. Three noise producing regimes were identified: (1) initial mixing layer between the outer stream and the ambient, (2) an interaction region for the primary and secondary mixing layers and (3) the fully merged regime downstream. For regime 1, the velocity and length scales were assumed to be the same as the outer stream velocity (U_2) and the outer nozzle diameter (D_o). For regime 2, they were assumed to be the primary stream velocity U_1 and a diameter such that the momentum conservation was satisfied. For regime 3, enthalpy conservation was also satisfied for heated flows,[7] with simplifying assumptions for unheated flows.[6] A prediction scheme synthesizing the noise from the three SEJ's quite successfully matched the coannular jet noise data. Here, we briefly review the assumptions for obtaining the SEJ parameters in the three regimes.

For regime 1, the choices of D_{eq}=D_o and U_{eq}=U_2 appear appropriate and supported by the congruence of the spectra on the high-frequency end. For regime 2 the equivalent diameter was defined as,

$$D_{eq} = D_1(1+\lambda^2\beta)^{1/2}, \qquad (9)$$

where, $\lambda = U_2 / U_1$ and $\beta = \rho_2 A_2 / \rho_1 A_1$. In Ref. 6, for regime 3, the following expressions were obtained with the simplifying assumption, $\rho_{eq} = \rho_1$,

$$D_{eq} = D_1(1+\lambda\beta)/(1+\lambda^2\beta)^{1/2} \qquad (10)$$

$$U_{eq} = U_1(1+\lambda^2\beta)/(1+\lambda\beta) \qquad (11)$$

In Ref. 7, enthalpy conservation was employed to obtain the following expressions for regime 3,

$$U_{eq} = U_1 \frac{(1+\lambda^2\beta'\delta)}{(1+\lambda\beta'\delta)}, \text{ and} \qquad (12)$$

$$D_{eq} = D_1\left[\frac{(1+\lambda\beta')(1+\lambda\beta'\delta)}{(1+\lambda^2\beta'\delta)}\right]^{1/2}, \qquad (13)$$

where, $\beta' = A_2 / A_1$ and $\delta = \rho_2 / \rho_1$.

The emphasis in Ref. 6 was on jets with normal velocity profiles where Eq. (9) applied well. We note that this definition may not apply for IVP jets, since in the limit $U_1 \rightarrow 0$, D_{eq} would be infinity. Derivation of D_{eq} and M_{eq} with equations (10) and (11) show good agreement with the constant enthalpy (red) curves of Fig. 4 for R<1, but significant difference occurs for R>1. Finally, with regards to equations (12) and (13), it is apparent that conservation of static enthalpy rather than total (stagnation) enthalpy was employed. In the format of equation (7) 'T' in Ref. 7 is static rather than total temperature. The parameters M_{eq} and D_{eq} obtained with equations (12) and (13) were found to be essentially the same in trend as seen in Figs. 4(a) and (b) (red curves); the amplitudes varied only slightly. Obviously, the differences did not pose a problem in the noise synthesis and could be absorbed in the correlation coefficients. However, it would be more rational to use the stagnation enthalpy conservation equation for regime 3 and, perhaps, also for regime 2.

3.4 Centerline Mach number data

Centerline data were obtained by Pitot-static probe surveys. Variations of static pressure for selected cases are shown in Fig. 11. The data exhibit sub-ambient pressures over a large range of axial distance. This phenomenon for single jets has been addressed in prior publications.[15,16] An increase in momentum flux, following regions of high turbulence intensities, is balanced by a drop in the static pressure. It is also seen that most of the cases start with a positive pressure near the nozzle that at first increases before dropping to negative values. At large R a negative pressure is encountered at the exit. As stated before, the limiting case of R=• has been excluded because the noise appeared abnormally high. This case was also marked by much lower negative pressures near the exit possibly due to a recirculation bubble occurring over the inner region.

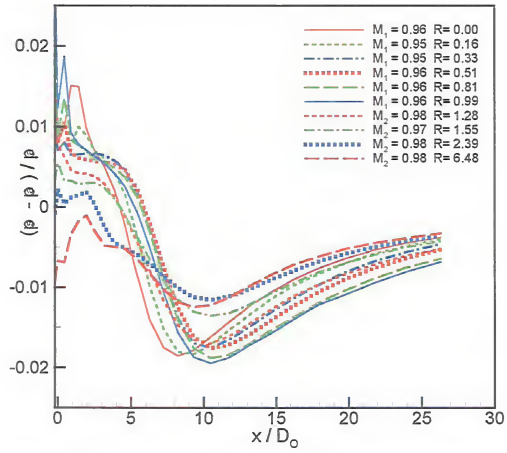

Fig. 11 Centerline variation of static pressure.

The static and Pitot pressures yielded the Mach number profiles. These are shown in Fig. 12(a) for the conditions of Fig. 11. For $R<1$, a lengthening of potential core can be noticed with increasing R.[17] For $R>1$, a peak occurs around $x/D_o = 5$, due to the fact that it takes some distance before the higher momentum annular flow gets mixed with the inner flow. The inverse of Mach number, normalized by SEJ parameters, is plotted in Fig. 12(b). We note that for R=0 and 0.99 (two solid curves) the results are close to each other, as expected, since each represents the single jet. For $R<1$ the curves are shifted downstream, the maximum shift occurring at $R = 0.5$. This shift appears to be simply due to the fact that M_{eq}/M starts with a value smaller than unity. For $R>1$, the curves are shifted upstream. Here, M_{eq}/M at first decreases to a minimum before increasing. The lowest value before the start of the increase is greater than unity causing the upstream shift of the curves. The asymptotic curves are found to be congruent for $R>1$but not for $R<1$; the reason remains unexplored.

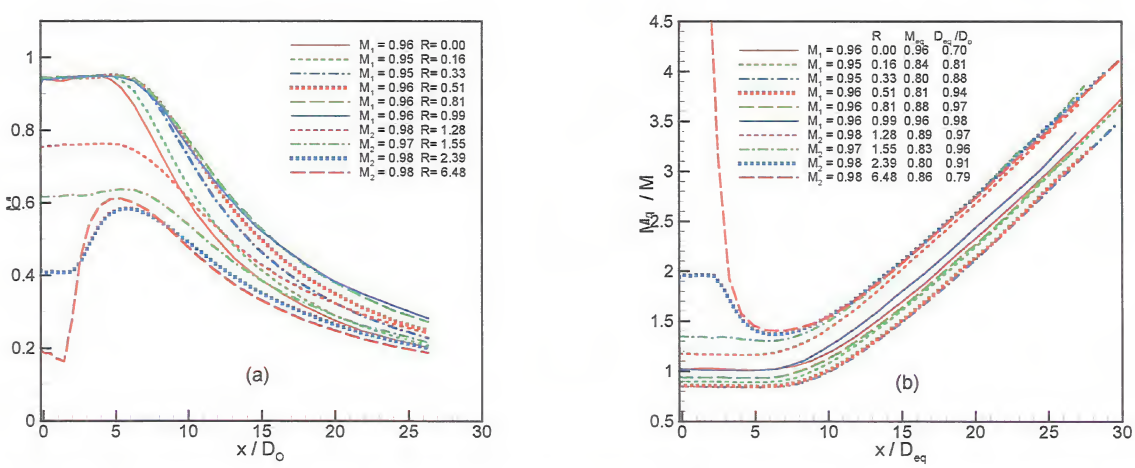

Fig. 12 Centerline variation of Mach number: (a) M versus x/D_o, (b) same data normalized by equivalent jet parameters.

The characteristics of the Mach number profiles are further analyzed in Figs. 13 and 14. The asymptotic slope is shown by the blue diamond symbols in Fig. 13. It is found to be about 0.14, close to but somewhat less than the value (0.16) noted in Ref. 18 for single jets. 'Potential core length' (x_p) is also plotted in Fig. 13. It is defined as the distance from the exit where the Mach number drops to 99% of the initial value. The data are not shown for $R>1$ since x_p is ill-defined in that regime. An increase in x_p with increasing R is seen clearly in Fig. 13. The upstream shift of the Mach number curves in Fig. 12(b) is reflected in the sharp decrease of x_p across R=1.

The potential core length data normalized by D_{eq} are shown in Fig. 14. For $R<1$, $x_p\ /D_{eq}$ turns out to be approximately constant at 6.5. We note here that in Ref. 17 $x_p\ /D_{eq}$ data were presented for coannular jets with fully expanded inner stream at $M_1 = 1.5$, for two bypass ratios. D_{eq} was defined simply based on conservation of mass

flux. A length $x_p / D_{eq} \approx 7$ was found for both cases that is comparable to the present data. Finally, the lateral shift of the M-curves of Fig. 12(b) is clearly captured by the 'virtual origin' (x_c) data shown by the blue symbols in Fig. 14. It is defined the same way as in Ref. 18 and represents the distance of the intersection of $M_{eq}/M = 1$ line with a radial line from the origin to a data point in the asymptotic region (at $x/D_{eq} = 25$). The abrupt shift across R=1 is clearly seen. The approximate value of $x_c/D_{eq} = 8$ at both R=0 and 1 agrees with the equation,

$$x_c / D_{eq} = 7.0 + 1.2 M_{eq}^{\ 2} + 1.2(1 - t_{eq} / T_a), \quad (14)$$

cited in Ref. 18. Overall, except for the virtual origin shift, the characteristics of the centerline Mach number decay agree well with single jet characteristics analyzed in Ref. 18.

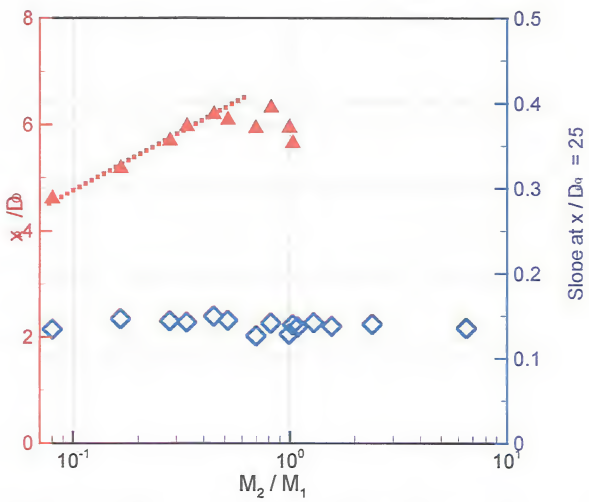

Fig. 13 Asymptotic slope at $x/D_{eq} = 25$ and 'potential core' length (x_p/D_o) from Mach number curves of Fig. 12.

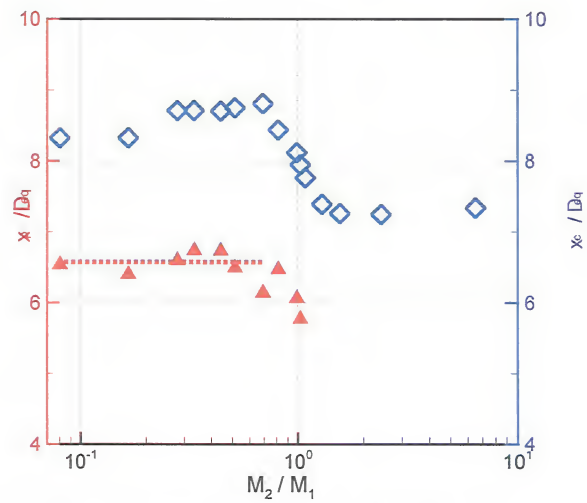

Fig. 14 'Potential core' length (x_p/D_{eq}) and 'virtual origin'(x_c/D_{eq}) from Mach number curves of Fig. 12.

4. Conclusions

Far-field noise and centerline Mach number decay data are documented in this paper for subsonic coannular jets. Scaling of the data is considered based on single equivalent jet parameters calculated by satisfying continuity, momentum and energy equations. The results confirm that coannular jets with 'normal' velocity profiles are noisier than the single equivalent jet. Jets with inverted velocity profiles are also found to be noisier except in a narrow range around R = 1.2. In the latter range while a few datasets display a hint of noise reduction, it is within the scatter of the data. Most datasets exhibit higher noise for the entire IVP range (R>1). Thus, for the parametric ranges covered in the present experiment, a single jet with top-hat velocity profile is found to be the quietest. Any nonuniformity introduced by the coannular configuration leads to a higher overall noise. When normalized with equivalent jet parameters the asymptotic Mach number decay rate, as well as potential core length, are found to be comparable to those of a single jet. However, discontinuities are observed around R=1. Specifically, an abrupt shift in the virtual origin is noted across this boundary.

Acknowledgement:
Support from the Quiet Aircraft Technology Program during the course of this study is gratefully acknowledged.

References:

1. Papamoschou D. and Debiasi, M., "Conceptual Development of Quiet Turbofan Engines for Supersonic Aircraft, *J. Propulsion and Power*, **19**(2), pp. 161-169, 2003.
2. Zaman, K.B.M.Q., "Noise- and flow-field of jets from an eccentric coannular nozzle", *AIAA Paper* 2004-0005, 42nd Aerospace Sciences Meeting, Reno, NV, January, 2004.
3. Williams, T. J., Ali, M.R.M.H. and Anderson, J.S., "Noise and flow characteristics of coaxial jets", *J. Mechanical Engineering Science*, **11**, pp. 133-142, 1969.

4. Tanna, H.K., "Coannular jets – are they really quiet and why?" *J. Sound & Vib.*, **72**(1), pp. 97-118, 1980.
5. Tanna, H.K. and Morris, P.J., "The noise from normal-velocity-profile coannular jets", *J. Sound & Vib.*, **98**(2), pp. 213-234, 1985.
6. Fisher, M.J., Preston, G.A. and Bryce, W. D., "A modeling of the noise from simple coaxial jets, part I: with unheated primary flow", *J. Sound and Vib.*, **209**(3), pp. 385-403, 1998.
7. Fisher, M.J., Preston, G.A. and Mead, C.J., "A modeling of the noise from simple coaxial jets, part II: with heated primary flow", *J. Sound and Vib.*, **209**(3), pp. 405-417, 1998.
8. Ko, N. W. M. and Kwan, A. S. H., "The initial region of subsonic co-axial jets", *J. Fluid Mechanics*, **73**, pp.305-332, 1976.
9. Pao, S. P., "A correlation of mixing noise from coannular jets with inverted flow profiles", *NASA TP* 1301, April, 1979.
10. Bridges, J. E. and Brown, C. A., "Validation of the Small Hot Jet Acoustic Rig for Aeroacoustic Research", 11th AIAA/CEAS Aeroacoustics Conf., Monterey, CA, 23-25 May, 2005 (submitted).
11. Viswanathan, K. and Clark, L., "Effect of nozzle internal contour on jet aeroacoustics", *AIAA Paper* 2004-0008, 42nd Aerospace Sciences Meeting, Reno, NV, January, 2004.
12. Zaman, K.B.M.Q. and Yu, J.C., "Power spectral density of subsonic jet noise", *J. Sound and Vib.,* **98**, pp. 519-537, 1985.
13. Bass, H.E., Sutherland, L.C., Zuckerwar, A.J., Blckstock, D.T. and Hester, D.M., "Atmospheric absorption of sound: further developments", *J. Acoust. Soc. Am.*, **97**(1), 1995.
14. Zaman, K.B.M.Q., "Effect of initial condition on subsonic jet noise", *AIAA J.,* **23**(9), pp. 1370-1373, 1985.
15. Hussain, A.K.M.F. and Clark, A.R., "Upstream influence on the near field of a plane turbulent jet", Physics of Fluids, 20, pp. 1416-1426, 1977.
16. Zaman, K.B.M.Q., "Flow field and near and far sound field of a subsonic jet", *J. Sound and Vib.*, **106**(1), pp. 1-16, 1986.
17. Murakami, E. and Papamoschou, D., "Mean flow development in dual-stream compressible jets", *AIAA J.*, **40**(6), pp. 1131-1138, 2002.
18. Zaman, K.B.M.Q., "Asymptotic spreading rate of initially compressible jets – experiment and analysis", *Physics of Fluids*, **10**(10), pp. 2652-2660, 1998.